

Baryon Form Factors at High Momentum Transfer and Generalized Parton Distributions

Paul Stoler

Physics Department, Rensselaer Polytechnic Institute, Troy, NY 12180

Abstract

Nucleon form factors at high momentum transfer t are treated in the framework of generalized parton distributions (GPD's). The possibility of obtaining information about parton high transverse momentum components by application of GPD's to form factors is discussed. This is illustrated by applying an *ad-hoc* 2-body parton wave function to elastic nucleon form factors F_1 and F_2 , the $N \rightarrow \Delta$ transition magnetic form factor G_M^* , and wide angle Compton scattering (WACS) form factor R_1 .

1 Introduction.

1.1 Valence PQCD.

One of the most studied questions relating to the properties of hadrons during the past decades has been how to describe exclusive reactions, and in particular electromagnetic form factors, in experimentally accessible regions of energy and momentum transfer. For momentum transfers of tens of GeV^2 , corresponding to characteristic wavelengths of less than 0.1 fm, ordinary constituent quark or flux tube models, which are a mainstay at much lower momentum transfers, appear to be inadequate, especially with increasing momentum transfer. Improved fits have been possible through modification of CQM's such as the introduction of quark form factors [1].

During the 1980's there was considerable theoretical progress in the description of exclusive reactions at asymptotically high momentum transfers in terms of the fundamental current quarks, applying valence perturbative QCD (PQCD), [2, 3, 4] together with SVZ [5] sum rules. Among the most important consequences of valence PQCD are the so called constituent counting rules, which predict relatively simple dependences of exclusive amplitudes as functions of momentum transfer. Many reactions experimentally appear to obey these constituent counting rules. Also, the magnetic nucleon elastic form factors and some resonant transition form factors could be roughly accounted for in magnitude through the application of the QCD sum rules [4, 6, 7, 8], leading to the possibility that valence PQCD would be applicable at kinematic conditions achieved at current or planned accelerator facilities. However, it had also been pointed out [9, 10] that the results of utilizing PQCD sum rules led to seemingly unrealistic valence quark longitudinal momentum fraction distributions $\phi(x)$. When utilized in the PQCD calculations, these $\phi(x)$'s led to inconsistent application of PQCD.

Another prediction of PQCD is hadron helicity conservation. Recent experiments [11, 12] at Jefferson Lab (JLab), which have measured helicity non-conserving amplitudes for elastic and resonance form factors, have shown that at momentum transfers approaching 6 GeV^2 the approach to PQCD is not manifest.

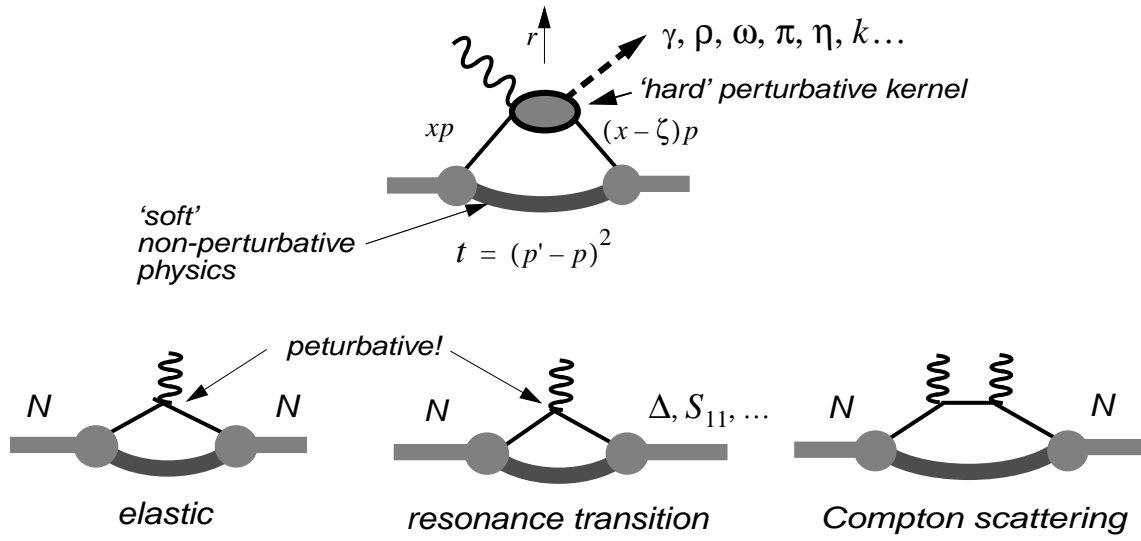


Figure 1: Diagrams representing the “handbag” mechanism; upper, deeply virtual Compton scattering and meson production; lower, nucleon elastic and resonance form factors, and wide angle Compton scattering.

1.2 Generalized Parton Distributions.

The recent evolution of the theoretical formalism of generalized parton distributions [13, 14, 15] (GPD’s) has shown promise of providing a framework for describing exclusive reactions in terms of parton degrees of freedom without invoking the internal hard mechanisms of valence PQCD. The GPD description has been discussed primarily in the reactions involving deeply virtual Compton scattering and meson production, at as high Q^2 and small t as possible. This is the kinematic region in which it has been shown that the reaction mechanism can be factorized into a hard perturbative, and soft non-perturbative part [15], the so-called *handbag* process illustrated in fig. 1.

The soft handbag is characterized by GPD’s which contain information about the distribution of quarks in the hadron. In particular, they give the amplitude that a quark with longitudinal momentum fraction x , in a hadron with momentum p , can be given a momentum kick $t = r^2$ with sideways component r_\perp , and re-absorbed by the hadron which emerges with a momentum $p - r$ (see fig. 1-top). Typically, hard electroproduction processes also require a longitudinal momentum transfer, characterized by a skewedness parameter $\zeta \equiv r_\parallel/p$. In the limit $t \rightarrow 0$ the certain GPD’s become identical with the deep inelastic scattering (DIS) structure functions, while others are not accessible in DIS.

A very important property of the GPD’s are sum rules which directly relate moments of the GPD’s to various hadronic form factors. For example, electron scattering form factors are the 0’th moments of the GPD’s.

For elastic scattering

$$F_1(t) = \int_0^1 \sum_q \mathcal{F}_\zeta^q(x, t) dx \quad (1)$$

$$F_2(t) = \int_0^1 \sum_q \mathcal{K}_\zeta^q(x, t) dx \quad (2)$$

where q signifies both quark and anti-quark flavors. We work in a reference frame in which the total momentum transfer is transverse so that $\zeta=0$, and denote $\mathcal{F}^q(x, t) \equiv \mathcal{F}_0^q(x, t)$, $\mathcal{K}^q(x, t) \equiv \mathcal{K}_0^q(x, t)$, etc.

For Compton scattering $\zeta = 0$, and the appropriate *form factor-like* quantities [16] are the -1'th moments of the GPD's

$$R_1(t) = \int_0^1 \sum_q \frac{1}{x} \mathcal{F}^q(x, t) dx \quad (3)$$

$$R_2(t) = \int_0^1 \sum_q \frac{1}{x} \mathcal{K}^q(x, t) dx \quad (4)$$

Resonance transition form factors access components of the GPD's which are not accessed in elastic scattering or WACS. The $N \rightarrow \Delta$ form factors are related to isovector components of the GPD's [17].

$$G_M^* = \int_0^1 \sum_q \mathcal{F}_M^q(x, t) dx \quad G_E^* = \int_0^1 \sum_q \mathcal{F}_E^q(x, t) dx \quad G_C^* = \int_0^1 \sum_q \mathcal{F}_C^q(x, t) dx \quad (5)$$

where G_M^* , G_E^* and G_C^* are magnetic, electric and Coulomb transition form factors [18], and \mathcal{F}_M^q , \mathcal{F}_E^q , and \mathcal{F}_C^q are axial (isovector) GPD's, which can be related to elastic GPD's in the large N_C limit through isospin rotations. Similar relationships can be obtained for the $N \rightarrow S_{11}$ and other transitions.

The GPD's as functions of x give the contributions to the form factors due to quarks of flavor q having momentum fraction x . As a function of t they are directly related to the perpendicular momentum distribution of partons in the hadron wave function in ways which are inaccessible to DIS. The Fourier transforms of the GPD's over r_\perp give the transverse impact parameter distributions [19].

In particular, at high $|t|$ the resulting baryon form factors are strongly related to the high momentum components of the valence quark distribution amplitudes. This is illustrated in the following sections, in which a simple *ad hoc* power behavior of the high k_\perp of the quark distribution is used.

2 Specific Examples.

2.1 Proton Dirac Form Factor F_1 .

The following is based on the development by Radyushkin [16], who calculated the proton helicity conserving form factor, F_1 , assuming that the handbag can be expressed as an effectively two-body process, as illustrated in fig. 2. The proton wave function is factorized as follows

$$\Psi(x, k_\perp) = \Phi(x) e^{-k_\perp^2/2x\bar{x}\lambda^2} \quad (6)$$

where $\bar{x} \equiv 1 - x$, and λ is a measure of the mean transverse momentum.

In terms of the two-body wave functions eq. (6), the form factors are then expressed as:

$$F^{tb} = \int \Psi^*(x, k_\perp + \bar{x}r_\perp) \Psi(x, k_\perp) \frac{d^2 k_\perp}{16\pi^3} \quad (7)$$

Comparing eqs. (7) and (1) gives

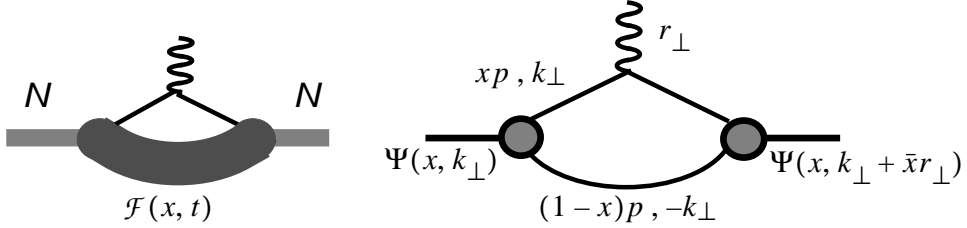


Figure 2: Schematic representation of the handbag mechanism as a two-body process.

$$\mathcal{F}(x, t) = \int_0^1 dx \int \Psi^*(x, k_\perp + \bar{x}r_\perp) \Psi(x, k_\perp) \frac{d^2 k_\perp}{16\pi^3} \quad (8)$$

Insertion of eq. (6) into eq. (8), and evaluating the integral then gives

$$\mathcal{F}(x, t) = \frac{x\bar{x}\lambda^2}{16\pi^2} \Phi^2(x) e^{-\bar{x}t/4x\lambda^2} \equiv f(x) e^{-\bar{x}t/4x\lambda^2} \quad (9)$$

with valence quark distributions

$$f(x) = \sum_q e_q f_q^v(x) = e_u f_u^v(x) + e_d f_d^v(x). \quad (10)$$

The functions $f_u(x)$ and $f_d(x)$ are chosen to agree with the valence quark distributions $f_q^v(x)$ obtained directly in DIS. In particular, ref. [16] uses an empirical function found to agree with DIS

$$f_u^v(x) = 1.89x^{-0.4}(1-x)^{3.5}(1+6x) \quad (11)$$

$$f_d^v(x) = 0.54x^{-0.6}(1-x)^{4.2}(1+8x). \quad (12)$$

The function $\Phi(x)$ in eq. (13) is then written

$$\Phi_q^2(x) = \frac{16\pi^2}{\lambda x \bar{x}} f_q^v(x). \quad (13)$$

Substitution of eqs. (10) and (13) into eq. (9), and then eq. (9) into eq. (1) yields for the proton Dirac form factor,

$$F_1(t) = \int_0^1 [e_u f_u^v(x) + e_d f_d^v(x)] e^{-\bar{x}t/4x\lambda^2} dx \quad (14)$$

The only free parameter in the analysis is λ , which is a measure of the mean k_\perp . A good fit to SLAC data for F_1 up to $|t| \sim 8$ GeV 2 was obtained. The resulting value of $\lambda^2 \sim 0.7$ GeV 2 leads to a reasonable values of the mean square k_\perp distributions: $\langle k_\perp^2 \rangle \sim (270\text{MeV})^2$

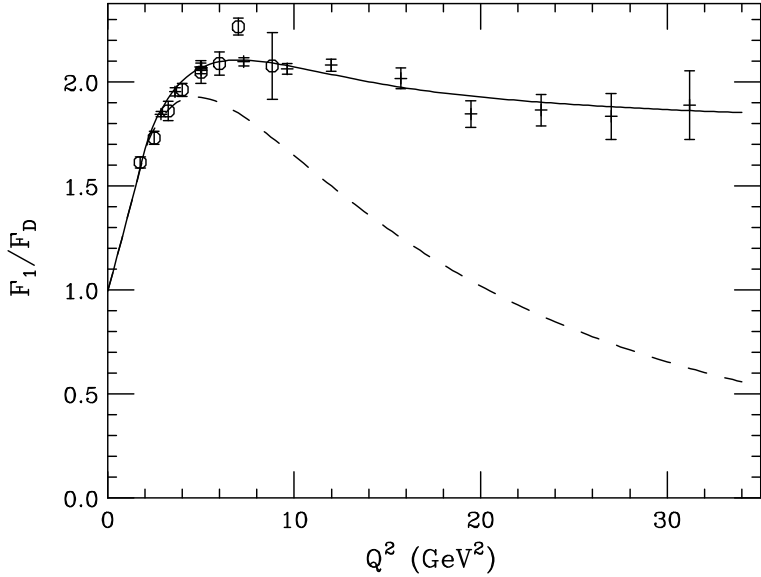


Figure 3: Proton Dirac form factor F_1 as a function of Q^2 . The data are from SLAC; circles (\circ) at lower Q^2 are from ref. [21], and pluses (+) at higher Q^2 are from ref. [20]. The dashed curve is the result of the soft wave function Ψ_{soft} . The solid curve is the result of adding a small hard component Ψ_{hard} .

2.2 Dirac Form Factor F_1 at High t

Data on F_1 exists [20] up to a Q^2 ($= -t$) of 32 GeV^2 . Continuation of the calculated F_1 to higher Q^2 exhibits a steadily greater discrepancy with the data with increasing Q^2 . This is shown in fig. 3.

A subsequent [22, 23] elaboration of the procedure of ref. [16] studied the relationship between model quark distribution amplitudes and form factors and Compton scattering. Ref. [22] used a valence quark distribution which evolves to the asymptotic form [3, 24], $\Phi(x) \rightarrow \Phi^{as}(x) \propto 120x_1x_2x_3$. In addition to the valence qqq configuration, higher Fock state contributions containing qqq, g and $qqq, \bar{q}q$ were added. For the k_\perp distribution, an exponential form similar to that in ref. [16] was used. For simplicity, the same λ^2 was used for all the three Fock state components, although the need to consider different λ^2 's for the valance and higher Fock states is discussed. It was found that the inclusion of the higher Fock states is significant, and can effect the form factors by as much as 20%. Overall the fit at higher Q^2 is improved, the fit at lower Q^2 somewhat deteriorated.

A Gaussian form of Ψ cannot account simultaneously for the F_1 magnitude and shape over the entire range of Q^2 . However, the addition of a small high k_\perp component in eq. (6) can dramatically improve the fit. As an example, we choose a *ad-hoc* $1/k_\perp^2$ behavior with lower cutoff parameter Λ , and upper cutoff $k_{\perp,max}$:

$$\Psi(x, k_\perp) = \Phi(x) \left(A_s e^{-k_\perp^2/2x\bar{x}\lambda^2} + A_h \frac{x\bar{x}\theta(k_\perp^2 < k_{\perp,max}^2)}{k_\perp^2 + \Lambda^2} \right) \equiv \Psi_{soft} + \Psi_{hard} \quad (15)$$

where $\lambda^2 = 0.7 \text{ GeV}^2$ is fixed by the low to intermediate Q^2 behavior of F_1 , $k_{\perp,max} = 4 \text{ GeV}^2$, and $\Lambda = 0.35 \text{ GeV}^2$. As seen in fig. 3, this small addition of Ψ_{hard} in eq. (15) can account for the high, as well as the low Q^2 magnetic form factor. A value of $A_h/A_s = 0.065$ was used in eq. (15)

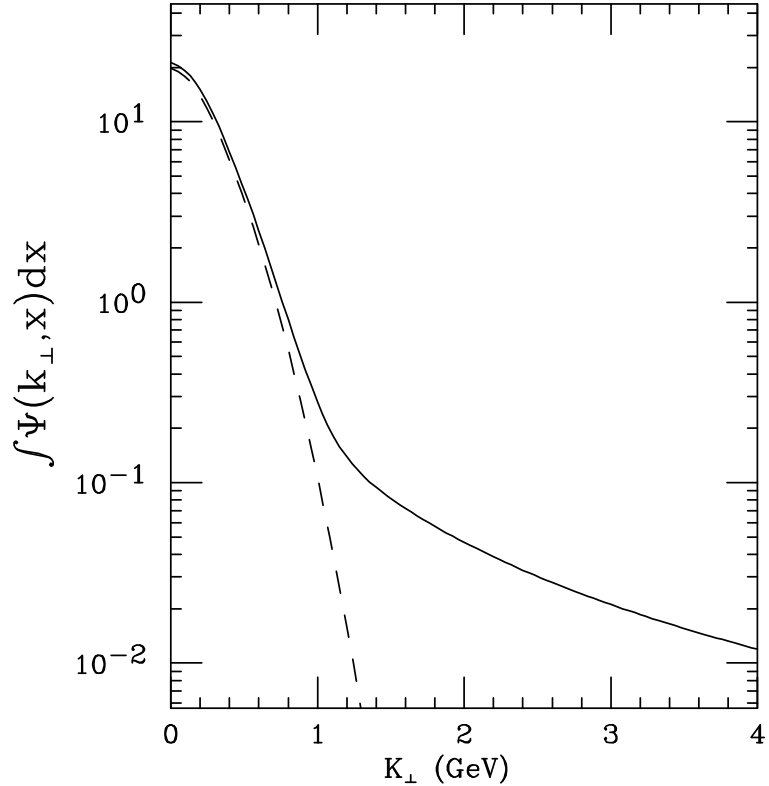


Figure 4: The function $\Psi(k_\perp) \equiv \int \Psi(x, k_\perp) dx$ vs. k_\perp . The dashed curve is due to the soft Gaussian component Ψ_{soft} , with $\lambda^2 = 0.7 \text{ GeV}^2$. The solid curve is $\Psi_{soft} + \Psi_{hard}$, with $A_h = 0.065$, $k_{\perp,max} = 4 \text{ GeV}$, and cutoff parameter $\Lambda = 0.35 \text{ GeV}$.

to obtain the solid curve. In all cases, the condition $\mathcal{F}(x, 0) = f(x)$ is maintained. Also, note that $F_1(0) = \int \mathcal{F}(x, 0) dx \approx 1$, which, is required in the definition of F_1 . The function $\Psi(k_\perp) = \int \Psi(k_\perp, x) dx$ is shown in fig. 4.

The resulting GPDs as a function of x for different values of t are shown in fig. 5. It would be interesting to see how this transforms into the spacial impact distributions $f(x, b_\perp)$ discussed in ref. [19].

Figure 6 shows the contribution to F_1 from different k_\perp regions. It is clear that the high Q^2 regions of F_1 are selective of the high components of $\Psi(k_\perp)$.

2.3 Pauli form factor F_2

Applying the analogous formalism as in ref. [16], Afanasev [25] modeled $\mathcal{K}(x, t)$ in eq. 2 as

$$\mathcal{K}^q(x, t) = k^q(x) e^{-\bar{x}t/4x\lambda^2}. \quad (16)$$

with λ and the normalization at $Q^2 = 0$ free parameters.

Unlike the case for $f^q(x)$, an expression for $k^q(x)$ cannot be obtained from DIS. Reference [25] notes that asymptotically PQCD and the SVZ sum rules require an extra factor of $1 - x$ for $k^q(x)$. In

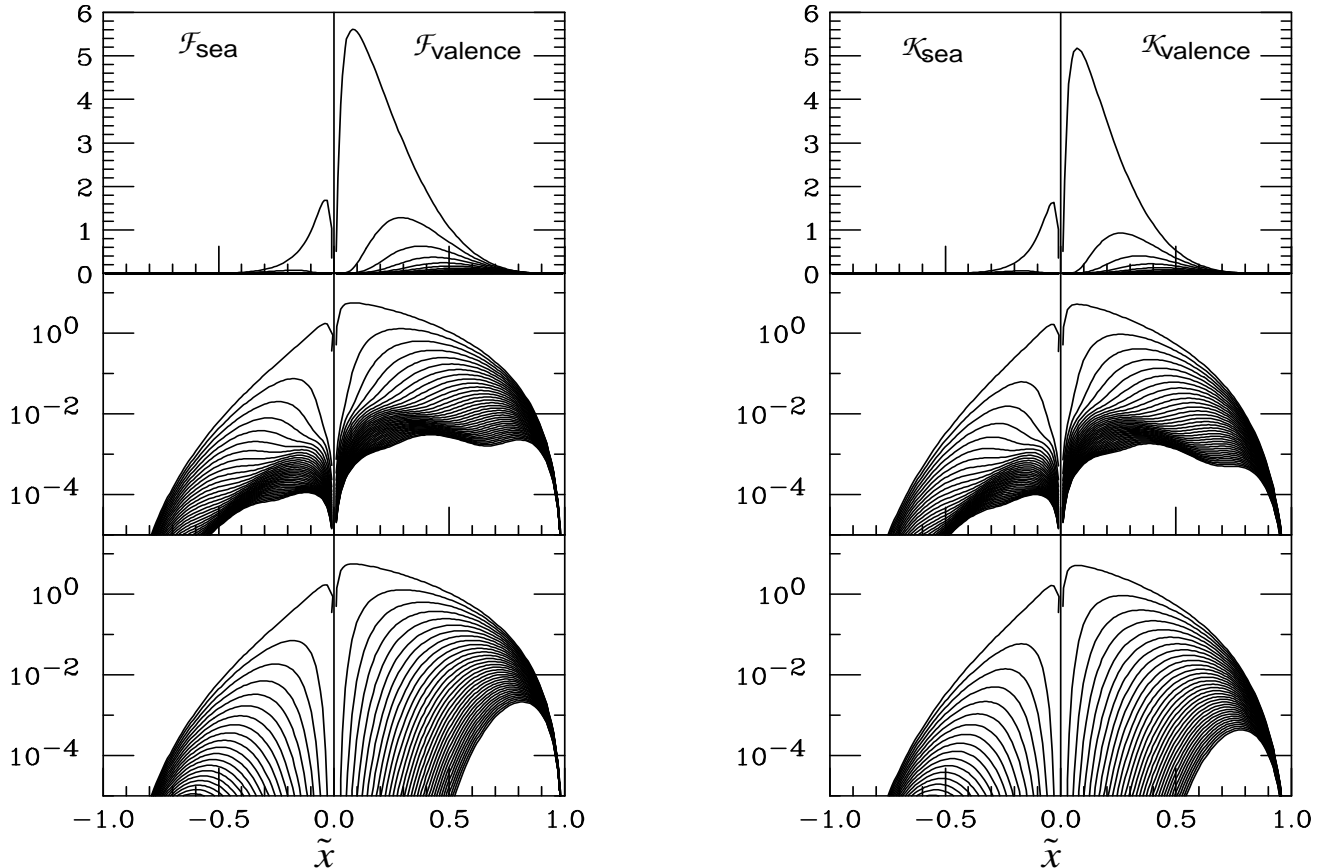


Figure 5: GPD's as a function of \tilde{x} for various values of t , where $\tilde{x} = x$ for valence quarks, and $\tilde{x} = -x$ for the sea quarks. The figures on the left and right are for \mathcal{F} and \mathcal{K} respectively. The graphs for positive \tilde{x} represent the *valence* quark contribution, while the graphs for negative \tilde{x} represent the *sea* quark contributions. The full GPDs are given by $\mathcal{F} = \mathcal{F}_{val} - \mathcal{F}_{sea}$ and $\mathcal{K} = \mathcal{K}_{val} - \mathcal{K}_{sea}$ respectively. The individual curves range from $|t| \sim 0 \text{ GeV}^2$ (highest curve in each panel) to $|t| = 35 \text{ GeV}^2$ (lowest curve in each panel). The upper and middle panels are the GPD's for the full wave function Ψ given in eq. (15), while those in the lowest panels are obtained using the soft wave function as in eq. (6). Note that the addition of the Ψ_{hard} mainly affects the GPD's at higher $|t|$ and $\tilde{x} < 0.5$.

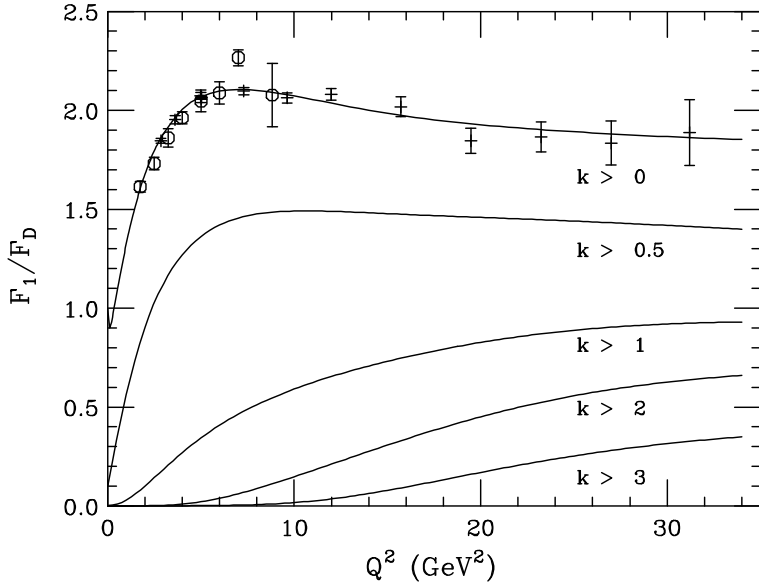


Figure 6: The contribution to F_1 from different regions in $\Psi(k_\perp)$ of k_\perp . Each curve represents the contribution from regions of k_\perp greater than the value indicated. The data are from SLAC; circles (\circ) at lower Q^2 are from ref. [21], and pluses (+) at higher Q^2 are from ref. [20].

the present study, it is found that the simplest form $k^q(x) = (1 - x)f^q(x)$ adequately describes the data. The expression for F_2 is then

$$F_2(t) = \int_0^1 [e_u k_u^v(x) + e_d k_d^v(x)] e^{-\bar{x}t/4x\lambda^2} dx \quad (17)$$

Figure 7 shows F_2 , and fig. 8 shows $Q^2 F_2(Q^2)/F_2(Q^2)$ compared with the recent JLab data [12]. The obtained G_{EP}/G_{MP} , also compared with the recent JLab data is shown in fig. 9. For F_2 the best fit was obtained for $\lambda^2 = 0.5$, and $F_2(0)$ was normalized to $\kappa = 1.79$. All other parameters, including A_H and Λ were fixed by F_1 . The contribution of Ψ_{soft} as in eq. (6) is also shown. The effects of inclusion of Ψ_{hard} become important at around $Q^2 = 8$ GeV 2 . The JLab upgrade includes measurements to about 15 GeV 2 , which should test this.

2.4 Wide angle Compton Scattering

The inclusion of Ψ_{hard} in eq. (15) also directly affects wide angle Compton scattering (WACS). Analogous to the elastic electron scattering form factors F_1 and F_2 are the Compton “form factors” R_1 and R_2 , which are related to the Klein-Nishina cross section:

$$\frac{d\sigma}{dt} = \left(\frac{d\sigma}{dt} \right)_{KN} R^2$$

with $R^2 = R_1^2(t) + \frac{-t}{4m_p^2} R_2^2(t)$. As in the case with electron scattering, $R_2(t)/R_1(t)$ is expected to fall as a power of $|t|$, so that the cross section at high $|t|$ is dominated by $R_1(t)$.

Since the integrals in R_1 and R_2 (eqs. (3, 4) are weighted with $1/x$, they may be expected to be more sensitive to the sea quark distribution. Reference [16] adds a sea quark contribution to $f_{Compton}$:

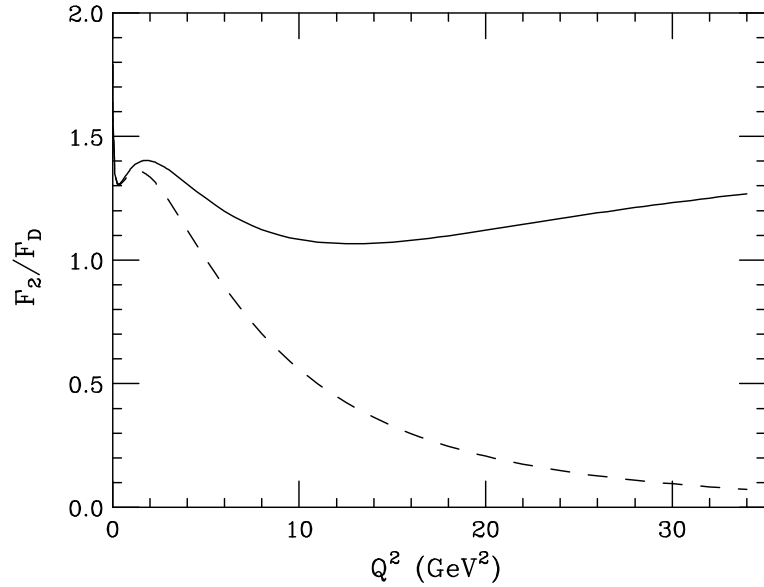


Figure 7: Proton Pauli form factor F_2 as a function of Q^2 . The dashed curve is the result of inclusion only of Ψ_{soft} in eq. (15). The solid curve is the result of adding Ψ_{hard}

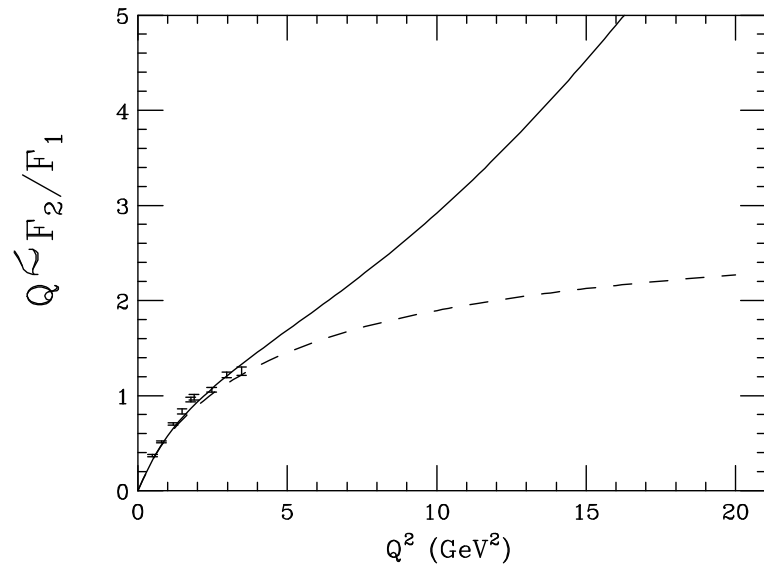


Figure 8: The ratio of the proton Dirac and Pauli form factors $Q^2 F_2 / F_1$ as a function of Q^2 . The dashed curve is the result of including only Ψ_{soft} . The solid curve is the result of adding Ψ_{hard} . The data are the recent JLab results [12].

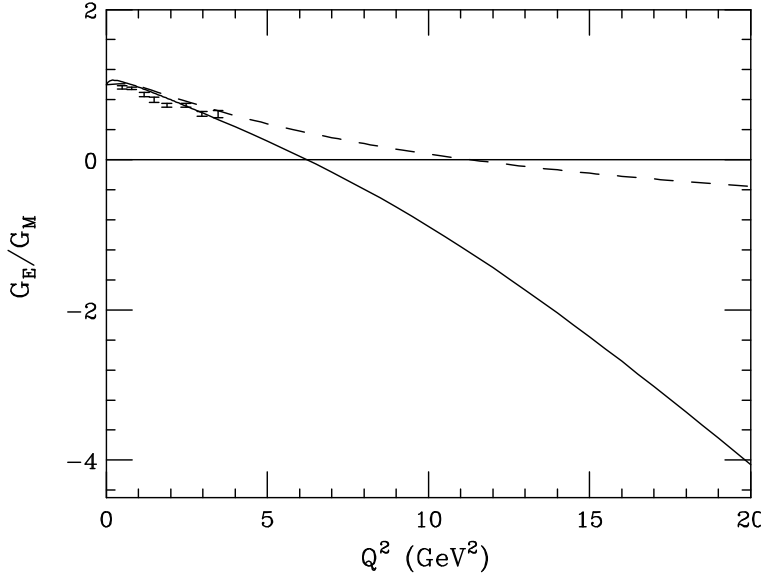


Figure 9: The ratio of the proton electric and magnetic form factors G_E/G_M as a function of Q^2 . The dashed curve is the result of inclusion only of Ψ_{soft} . The solid curve is the result of adding Ψ_{hard} . The data are the recent JLab results [12]

$$f_{Compton} = f_{Compton}^{val} + f_{Compton}^{sea}$$

with

$$f_{Compton}^{val} = e_u^2 f_u^v(x) + e_d^2 f_d^v(x)$$

and

$$f_{Compton}^{sea} = (e_u^2 + e_d^2 + e_s^2) f^{sea}(x)$$

where f_u^v and f_d^v are parameterized as in eqs. (11) and (12), respectively, and $f^{sea}(x)$ is parameterized as follows:

$$f^{sea}(x) = 0.5x^{-0.75}(1.0 - x)^7$$

Figure 10 shows the result for $R_1(t)$ with and without the presence of Ψ_{hard} . All parameters in Ψ_{soft} and Ψ_{hard} are fixed by the fit to $F_1(Q^2)$. The proposed experiments at JLab with a 12 GeV electron beam are expected to reach $|t| = 15$ GeV 2 , and therefore should be sensitive to the consistency of the approach. Figure 11 shows the contribution to R_1 from different k_\perp regions of $\Psi(k_\perp)$. It is clear that the high $|t|$ regions of R_1 are selective of the high components of $\Psi(k_\perp)$.

Reference [22] have also evaluated wide angle Compton scattering, and find the higher Fock components contribute an even more significant fraction of the form factors (R_1, R_2) than in elastic scattering, especially at lower $|t|$, as may be expected.

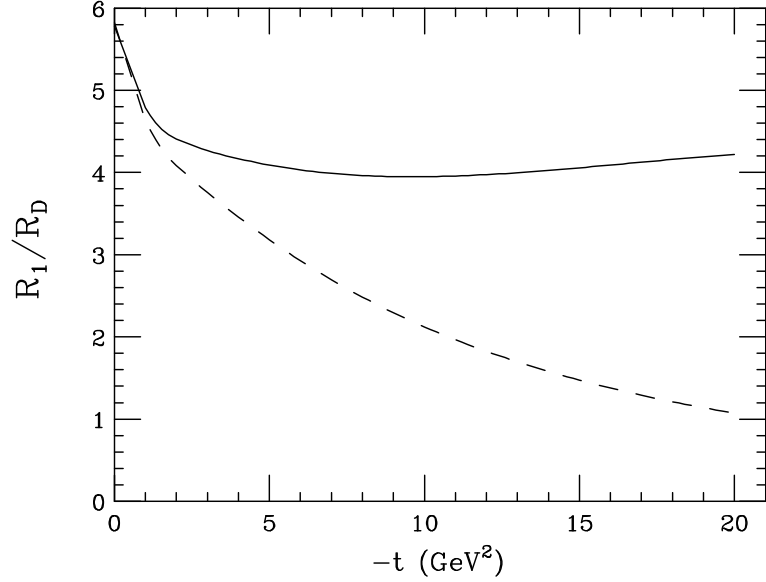


Figure 10: The Compton form factor $R_1(t)$ vs. t , using $\Psi = \Psi_{soft}$ (dashed) and $\Psi = \Psi_{soft} + \Psi_{hard}$ (solid).

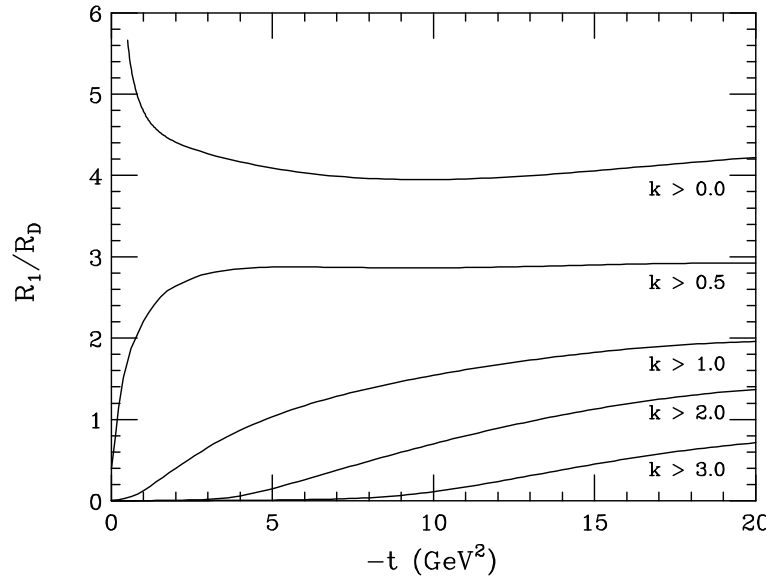


Figure 11: The contribution to R_1 from different regions in $\Psi(k_\perp)$ of k_\perp . Each curve represents the contribution from regions of k_\perp greater than the value indicated.

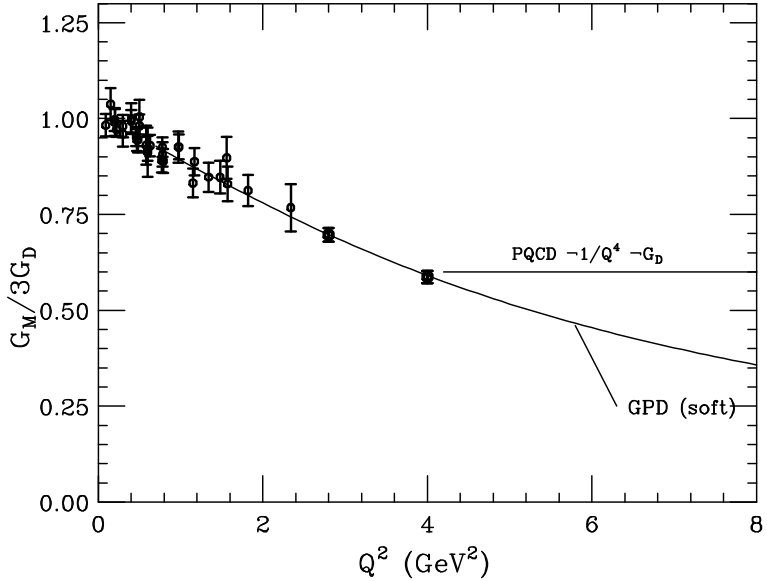


Figure 12: The $N \rightarrow \Delta$ magnetic form factor $G_M^*(Q^2)$ relative to the dipole $G_D = 3/(1 + 0.71Q^2)^2$. The data points for Q^2 below 2.8 GeV^2 are from a compilation of ref. [26]. Those at $Q^2 = 2.8$ and 4.0 GeV^2 are recent JLab data [11]. The horizontal line reflects the $1/Q^4$ asymptotic PQCD shape, and the curve denoted GPD is discussed in the text.

2.5 $N \rightarrow \Delta$ transition.

The transition $N \rightarrow \Delta(1232)$ is purely isovector, which can be expressed in terms of three transition form factors [18]; magnetic $G_M^*(Q^2)$, electric $G_E^*(Q^2)$, and Coulomb (or scalar) $G_C^*(Q^2)$, with $(p_\Delta - p)^2 = t = -Q^2$. These can be expressed in terms of the isovector components of the GPD's [17]:

$$\begin{aligned} G_M^*(t) &= \int_0^1 \sum_q \mathcal{F}_M^{(3)q}(x, t) dx \\ G_E^*(t) &= \int_0^1 \sum_q \mathcal{F}_E^{(3)q}(x, t) dx \\ G_C^*(t) &= \int_0^1 \sum_q \mathcal{F}_C^{(3)q}(x, t) dx \end{aligned}$$

The experimental status of the $N \rightarrow \Delta$ transition magnetic form factor is shown in figure 12. The decrease in G_M^* relative to G_D indicates that the transition form factor is softer than that for elastic scattering. The soft part of the transition form factor can be modeled by assuming a different λ parameter for Ψ_Δ than Ψ_P . Thus, we take

$$\Psi_{P,soft}(x, k_\perp) = \Phi_P(x) e^{(-k_\perp^2/2x\bar{x}\lambda_P^2)}$$

$$\Psi_{\Delta,soft}(x, k_\perp) = \Phi_\Delta(x) e^{(-k_\perp^2/2x\bar{x}\lambda_\Delta^2)}$$

For simplicity we have taken $\Phi_\Delta(x) = \Phi_P(x) = \Phi(x)$. This leads to

$$F_{N\Delta}(x, k_\perp, t) = \frac{x\bar{x}}{8\pi^2} \left(\frac{\lambda_P^2 \lambda_\Delta^2}{\lambda_P^2 + \lambda_\Delta^2} \right) \Phi^2(x) e^{-\frac{\bar{x}|t|}{2x} \left(\frac{1}{\lambda_P^2 + \lambda_\Delta^2} \right)}.$$

The curve passing through the data is obtained with $\lambda_{P\Delta}^2 \equiv \lambda_P^2 + \lambda_\Delta^2 = 0.38$ implying a transition $(k_\perp)_{RMS} \sim (180)^2$ (MeV)², which is considerably smaller than the value obtained for elastic scattering from the proton. This also implies that the mean transition radius for the $N \rightarrow \Delta$ transition is also larger than for proton elastic scattering.

3 Conclusion.

The advent of the GPD formalism offers a framework to model the k_\perp distributions of quarks which are involved in exclusive reactions. These distributions are constrained by providing simultaneous fits to several different reactions rather than by fitting form factors for a single specific reaction. Furthermore, specific reactions may be sensitive to specific components of GPD. For example the $N \rightarrow \Delta$ is selective of isovector components.

Within the two-body framework presented, high Q^2 (or $|t|$) form factors are sensitive to the high momentum components of the underlying wave functions. The sensitivities become significant at Q^2 or $|t|$ greater than about 7 or 8 GeV². Currently, only G_{MP} experimental data extend to much higher values of Q^2 . However, the proposed program of high $|t|$ exclusive measurements for the Jefferson Lab 12 GeV upgrade is anticipated to provide high quality data for all of the reactions discussed here.

The example given here for modeling the *hard* part of the wave function is purely *ad-hoc* and not meant as a rigorous theoretical procedure, but indicative of the sensitivity of high $|t|$ exclusive reactions to high momentum components of the nucleon parton distribution. More rigorous theoretical approaches are expected in parallel with the high quality data expected in the future.

Acknowledgements:

The author thanks Anatoly Radyushkin for much discussion and guidance. Richard Davidson is thanked for helpful discussions.

The work was partially supported by the *National Science Foundation*.

References

- [1] F. Cardarelli et al., *Physics Letters* **B371**, 7 (1996)
- [2] A.V. Efremov and A.V. Radyushkin, *Theor. Math. Phys.* **42**, 97 (1980)
- [3] S. J. Brodsky and G. P. Lepage, *Phys. Rev.* **D22**, 2157 (1980).
- [4] V.L. Chernyak and I.R. Zhitnitsky, *Physics Reports*, **112**, 173 (1984).
- [5] M.A. Shiffman, A.I. Vainstein and V.I.Zakharov, *Nuc. Phys.*, **B47**, 385, 448, 519 (1979).
- [6] C. E. Carlson and J. L. Poor, *Phys. Rev.* **D38**, 2758 (1988).
- [7] P. Stoler, *Physics Reports* **226**, 103 (1993).

- [8] G. Sterman and P. Stoler, Annual Reviews of Nuclear and Particle Science, **47**, 193 (1997).
- [9] A. V. Radyushkin, *Nucl. Phys.* **A527**, 153c (1991).
- [10] N. Isgur and C. H. Lewellyn- Smith, *Phys. Rev. Lett.* **52**, 1080 (1984);
- [11] V. V. Frolov, PhD thesis, Rensselaer Polytechnic Institute; V. V. Frolov, *et al.* *Phys. Rev. Lett.* **82**, 45 (1999).
- [12] M.K. Jones *et al.* *Phys. Rev. Lett.* **84**, 1398 (2000).
- [13] X. Ji, *Phys. Rev. Lett.* **78**, 610 (1997);
- [14] A. Radyushkin, *Phys. Lett.* **B380**, 417 (1996); *Phys. Rev.* **D56**, 5524 (1997).
- [15] J. Collins, L. Frankfort, and M. Strikman, *Phys. Rev.*, **D56**, 2982 (1997).
- [16] A. Radyushkin, *Phys. Rev.* **D58**, 114008 (1998).
- [17] K. Goeke, M.V. Polyakov, and M. Vanderhaeghen, Preprint hep-ph/01060112, 1 June, (2001)
- [18] H.F. Jones and M.D. Scadron, *Annals of Physics* **81**, 1 (1979).
- [19] *Phys. Rev.* **D62**, 0701503 (2000); hep-ph/0005108.
- [20] R.G. Arnold *et al.*, *Phys. Rev. Lett.* **57**, 174 (1986).
- [21] L. Andihavis *et al.*, *Phys. Rev.* **D50**, 5491 (1994).
- [22] M. Diehl, Th. Feldmann, R. Jakob and P. Kroll, *Eur. Phys. J.* **C8**, 409 (1999); hep-ph/9811253.
- [23] M. Diehl, Th. Feldmann, R. Jakob and P. Kroll, *Nucl. Phys.* **B596**, 33 (2001), Erratum-*ibid.* **B605**, 647 (2001); hep-ph/0009255.
- [24] J. Bolz and P. Kroll, *Z. Phys.* **A356**, 327 (1996).
- [25] A. Afanasev, E-print: hep-ph/9910565; “Proceeding of the JLAB-INT Workshop on Exclusive and Semi-Exclusive Processes at High Momentum Transfer”, C. Carson and A. Radyushkin, eds. World Scientific (2000). May 1999
- [26] S.S. Kamalov and S. N. Yang, *Phys. Rev. Lett.* **83**, 4494 (1999).